Low-Temperature Growth of Graphene on a Semiconductor

Røst, Hakon I.; Chellappan, Rajesh Kumar; Strand, Frode S.; Grubisic-Cabo, Antonija; Reed, Benjamen P.; Prieto, Mauricio J.; Tanase, Liviu C.; De Souza Caldas, Lucas; Wongpinij, Thipusa; Euaruksakul, Chanan; Schmidt, Thomas; Tadich, Anton; Cowie, Bruce C.C.; Li, Zheshen; Cooil, Simon P.; Wells, Justin W.

Published in:
Journal of Physical Chemistry C

DOI:
10.1021/acs.jpcc.0c10870

Publication date:
2021

Citation for published version (APA):
Røst, H. I., Chellappan, R. K., Strand, F. S., Grubisic-Cabo, A., Reed, B. P., Prieto, M. J., Tanase, L. C., De Souza Caldas, L., Wongpinij, T., Euaruksakul, C., Schmidt, T., Tadich, A., Cowie, B. C. C., Li, Z., Cooil, S. P., & Wells, J. W. (2021). Low-Temperature Growth of Graphene on a Semiconductor. *Journal of Physical Chemistry C*, *125*(7), 4243-4252. https://doi.org/10.1021/acs.jpcc.0c10870

THE JOURNAL OF PHYSICAL CHEMISTRY C
A JOURNAL OF THE AMERICAN CHEMICAL SOCIETY

pubs.acs.org/JPCC

Article

Low-Temperature Growth of Graphene on a Semiconductor

Håkon I. Røst,* Rajesh Kumar Chellappan,* Frode S. Strand, Antonija Grubišić-Čabo, Benjamen P. Reed, Mauricio J. Prieto, Liviu C. Tănase, Lucas de Souza Caldas, Thipusa Wongpinij, Chanan Euaruksakul, Thomas Schmidt, Anton Tadich, Bruce C. C. Cowie, Zheshen Li, Simon P. Cooil, and Justin W. Wells*

Cite This: *J. Phys. Chem. C* 2021, 125, 4243−4252

Read Online

ACCESS | Metrics & More | Article Recommendations | Supporting Information

ABSTRACT: The industrial realization of graphene has so far been limited by challenges related to the quality, reproducibility, and high process temperatures required to manufacture graphene on suitable substrates. We demonstrate that epitaxial graphene can be grown on transition-metal-treated 6H-SiC(0001) surfaces, with an onset of graphitization starting around 450−500 °C. From the chemical reaction between SiC and thin films of Fe or Ru, sp^3 carbon is liberated from the SiC crystal and converted to sp^2 carbon at the surface. The quality of the graphene is demonstrated by using angle-resolved photoemission spectroscopy and low-energy electron diffraction. Furthermore, the orientation and placement of the graphene layers relative to the SiC substrate are verified by using angle-resolved absorption spectroscopy and energy-dependent photoelectron spectroscopy, respectively. With subsequent thermal treatments to higher temperatures, a steerable diffusion of the metal layers into the bulk SiC is achieved. The result is graphene supported on magnetic silicide or optionally, directly on semiconductor, at temperatures ideal for further large-scale processing into graphene-based device structures.

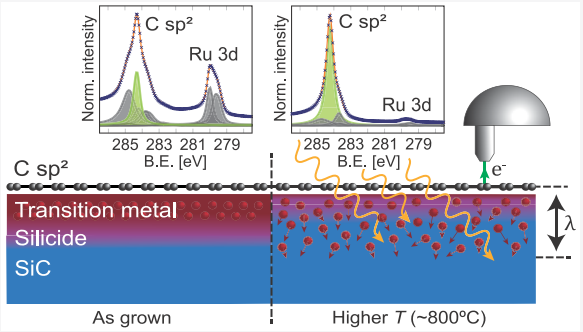

INTRODUCTION

Since its experimental discovery in 2004,[1] graphene—a two-dimensional carbon crystal in a honeycomb structure—has been deemed a promising candidate for device applications because of its exceptional electronic, thermal, optical, and mechanical properties.[2−6] However, the challenges associated with the production of large-scale high-quality graphene layers directly on semiconductor substrates have limited the integration of graphene with conventional device prototypes.

Until now, the most common techniques for preparing monolayer graphene include micromechanical exfoliation from bulk graphite, epitaxial growth on various transition metals[7−10] through chemical vapor deposition (CVD) of hydrocarbons, and thermal decomposition of bulk crystals such as silicon carbide.[11,12] Among these methods, epitaxial growth by CVD and thermal decomposition of SiC are normally favored as large-area single-crystalline graphene domains can be achieved routinely.[13−15] However, CVD grown graphene requires an additional transfer step onto a suitable substrate, limiting the scalability of the technique when it comes to producing graphene on a semiconductor or dielectric of uniform size and quality. The transfer may also introduce contaminants and affect the quality of the CVD graphene, compromising its suitability for device integration.[16] In comparison, graphene prepared on SiC can be directly converted into a device,[17] but the temperatures needed to trigger the thermal decomposition of the SiC are by far incommensurate with those of device industry standards.[18]

In this study, we demonstrate how catalytic reactions between SiC surfaces and thin films of transition metals Fe and Ru can produce quasi-freestanding graphene layers at significantly lower temperatures than those of "conventional" epitaxial growth. Surface graphene layers are formed by allowing the thermally activated metal films to convert sp^3 carbon from the substrate into sp^2 carbon, which re-forms at the surface. A similar method has previously been successfully demonstrated at temperatures of 500−600 °C by using Fe on both SiC and diamond.[19,20] Here, we show that ordered graphene layers can be produced from SiC by using either Fe or Ru, with an onset of growth starting at around 450−500 °C. This metal-mediated approach leaves graphene resting on underlying layers of metal silicide, which can then be eliminated by subsequent thermal treatments to higher temperatures, driving diffusion of the metal ions into the bulk crystal.[21] The result is quasi-freestanding graphene resting

Received: December 4, 2020
Revised: January 27, 2021
Published: February 9, 2021

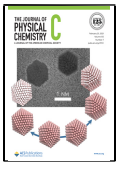

https://dx.doi.org/10.1021/acs.jpcc.0c10870
J. Phys. Chem. C 2021, 125, 4243−4252

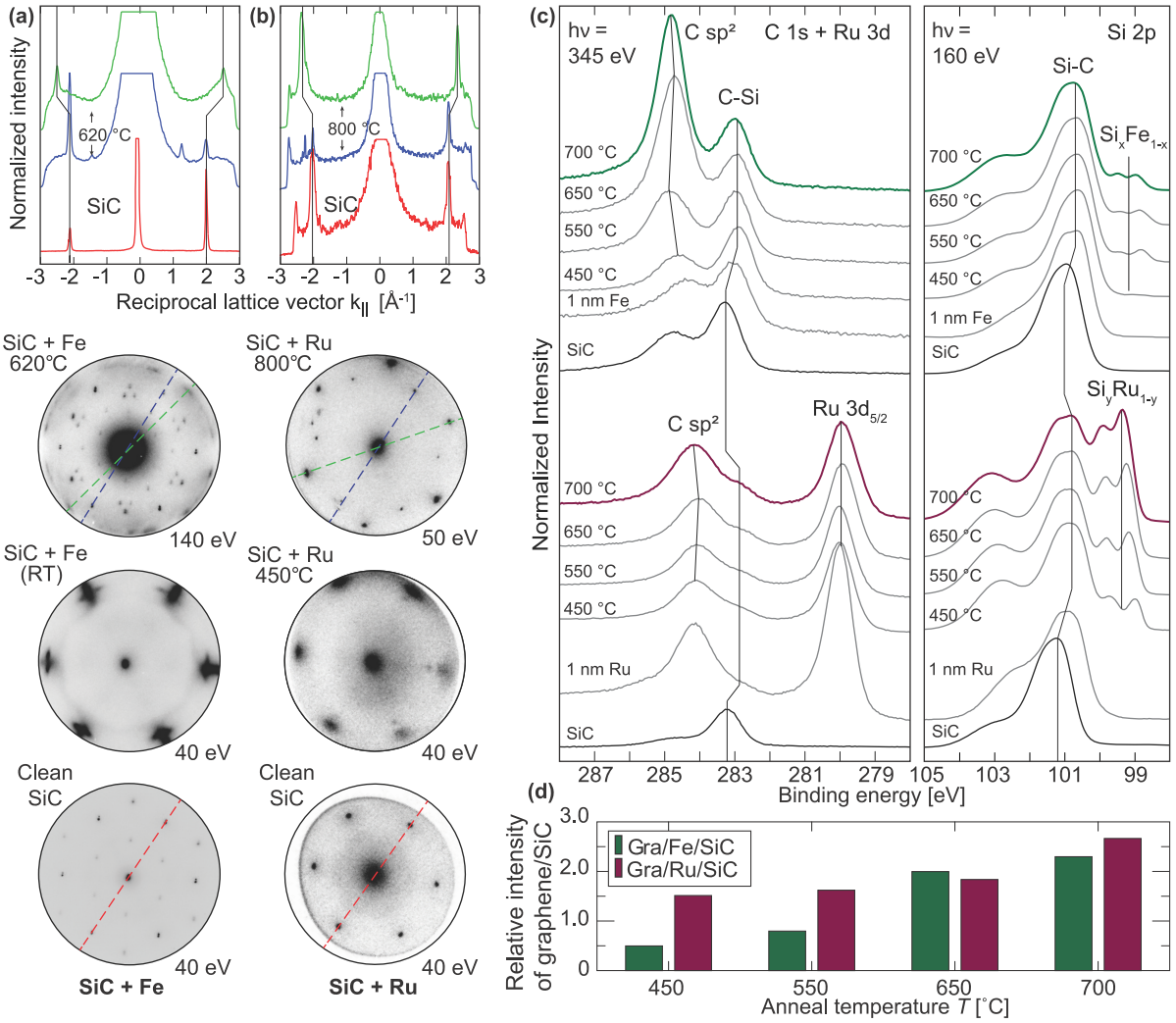

Figure 1. Gradual formation of graphene on SiC treated with Fe and Ru. (a, b) μ-LEED patterns of 6H-SiC coated with thin films of Fe and Ru, respectively, and then thermally treated to temperatures of 600−800 °C. The excitation energy/starting voltages were adjusted for the final images to increase the brightness of all relevant spots. Intensity cuts along high-symmetry directions of the reciprocal lattices of the two systems (topmost panels) reveal new diffraction maxima appearing with the formation of graphitic carbon at the surface. These appear at angles 30° (SiC + Ru) as well as 15° and 45° (SiC + Fe) relative to the (1 × 1) phase of the underlying SiC. All intensity cuts were normalized to the **k** values and intensities of the first-order SiC spots. (c) Core levels Si 2p, C 1s, and Ru 3d showing the formation of graphitic layers: silicon carbide, followed by deposition of Fe and Ru and successive thermal treatments in the range 450−700 °C. All core levels have been normalized to the intensity of the SiC signal ("C−Si" and "Si−C"). (d) Estimated ratio of graphitic carbon to silicon carbide signal measured within a few nanometers of the surface as a function of temperature.

on semiconducting substrates and grown at industrially compatible temperatures, ideal for further processing into large-scale, graphene-based device structures.

METHODS

Single crystal samples of n-type 6H-SiC(0001) (Tankeblue Semiconductor) were initially cleaned *ex situ* by using standard "RCA" chemical cleaning procedures to remove residual contaminants and native oxides.[22] The samples were then loaded into the relevant spectrometers and degassed *in situ* at 300 °C in ultrahigh vacuum (UHV) for durations of 6+ h. Finally, any residues of silicon oxide on the surfaces were removed by rapidly annealing each sample to roughly 900 °C for several cycles. Because of different heating setups for the different spectrometers, temperature differences of ±50 °C were achieved during the flashing. The preparation of clean 6H-SiC(0001) was confirmed by using X-ray photoelectron spectroscopy (XPS) and low-energy electron diffraction (LEED). In each experimental setup, several different samples were loaded, cleaned, and compared. Slight variations in the XPS and reconstructions of the clean surface were observed; however, neither appeared to have any significant impact on the subsequent growth steps.

Fe and Ru films with different thicknesses in the range 0.5−2.0 nm were deposited on individual samples at constant rate by using calibrated e-beam evaporation cells. The transition-metal-covered samples were then annealed for short durations at increasing temperatures ranging from 450 to 700 °C to study the formation of transition metal (TM) silicides, the associated liberation of carbon atoms and the sp^2 reconstruction at the surface. The homogeneity of the metal films and the graphitic surface layers was verified across ranges of 500 μm by using low-energy electron diffraction (LEEM) and X-ray photoemission electron microscopy (XPEEM). Small-spot

https://dx.doi.org/10.1021/acs.jpcc.0c10870
J. Phys. Chem. C 2021, 125, 4243−4252

low-energy electron diffraction (μ-LEED) was recorded from selected areas of 1.5 μm diameter within the same regions at every relevant preparation stage. Following graphene formation, small-spot angle-resolved photoemission spectroscopy (μ-ARPES) was extracted from diffractive plane measurements of the Fe/SiC system, also from areas of 1.5 μm diameter.

Subsequent annealing to 800 °C for a longer duration was performed on some samples to further study the thermally activated graphitization and to investigate any associated changes to the concentration level of metal in the surface layers. Measurements were performed both prior to and following the thermal treatments to monitor the change with every experimental step. The formation of additional silicides and sp^2 carbon was confirmed through photon-energy-dependent XPS measurements of the Si 2p and C 1s core levels and, where possible, NEXAFS measurements of the C 1s K-edge.

RESULTS AND DISCUSSION

The gradual formation of graphitic carbon at the surface of Fe/SiC and Ru/SiC as a function of temperature is illustrated in Figure 1. Chemically and thermally cleaned SiC crystals treated with thin films of Fe and Ru were studied after metallization and subsequent annealing to higher temperature by small-spot low-energy electron diffraction (μ-LEED) and high-energy-resolution X-ray photoelectron spectroscopy (XPS).

The developments of the surface diffraction patterns originating from the two systems are shown in Figures 1a and 1b. Following the initial high-temperature annealing, both samples display known surface reconstructions of the SiC(0001) face: namely, a (1×1) phase and a $(\sqrt{3} \times \sqrt{3})R30°$ silicate reconstruction.[23] Both indicate a clean surface devoid of excessive oxide, the latter being the result of a higher flash temperature toward 1000 °C.[24,25] From our investigations, both reconstructions of the initial surface have been observed to yield similar results in the successive growth steps.

With metallization, the additional Fe and Ru layers both seem to mimic the hexagonal arrangement of the Si atoms with a slight lattice mismatch: the newfound diffraction spots both appear at larger magnitudes of the momentum wave vector $\mathbf{k}$ than the first-order SiC spots. Note that while the Fe film crystallizes already at room temperature, the Ru needs an additional thermal treatment to 450 °C to order itself with similar quality on top of the SiC. The different crystallization energies required for the two metal films are believed to be related to their different structural mismatch with the SiC(0001) surface.

Upon thermal activation above 600 °C, the metallic spots disappear, and the original (1×1) phase of the SiC(0001) face again becomes visible, as seen from comparing the intensity profiles along the same high symmetry direction for the clean SiC (red dashed line) and after the thermal treatments (blue dashed line). The recurrence of the SiC pattern is also accompanied by several new diffractive features, some of which are similar to previous reports of the Fe/SiC system.[19] Notably, both systems show higher $\mathbf{k}$ features appearing at rotations 15° and 45° (Fe) or 30° (Ru) relative to the SiC spots. Investigating these more closely along their symmetry directions (green dashed line) and comparing them to the simultaneously visible SiC features reveal that the new spots occur at $|\mathbf{k}| \sim 2.36$ Å^{-1} for Ru/SiC and $|\mathbf{k}| \sim 2.50$ Å^{-1} for Fe/SiC. Both values are within 10% of the $|\mathbf{k}|$ value associated with pristine graphene flakes of lattice constant $a = 2.46$ Å.[26]

At first glance, the newfound spots on Ru/SiC in Figure 1b could be interpreted to come from the SiC surface, as their $|\mathbf{k}|$ value is similar to the second-order spots of a $(\sqrt{3} \times \sqrt{3})R30°$ silicate reconstruction. However, no first-order spots from this reconstruction are observed, and hence the $|\mathbf{k}| \sim 2.36$ Å^{-1} spots cannot be explained from the SiC surface alone. Also, the different $|\mathbf{k}|$ values and relative orientation of newfound surface layers on Fe/SiC and Ru/SiC are not surprising: both may well be explained from different interactions with Fe and Ru. Each new layer is expected to be ordered according to its underlying metal, which again should be oriented to minimize its lattice mismatch with the SiC(0001). Given the structural differences between Fe and Ru, variations in strain and rotation for the new surface layer are not unlikely.

The C 1s and Si 2p core levels for both material systems, from samples with similar preparation, are shown in Figures 1c and 1d. Both regions were acquired from photoelectrons with a shallow escape depth ($\lambda \sim 0.5$ nm) beneath the sample surface. Similar features indicative of clean SiC can be seen for both systems: dominant peak components from the Si−C bonding of the substrate can be found at binding energies 283.2 eV (C 1s) and 101.2 eV (Si 2p), with minor features at 284.8 and 103.5 eV, indicating some occurrence of C−C bonding[27,28] and silicon oxide formation.[29,30] Note that slight variations in the initial amount of C−C and silicon oxide can be seen from the XPS measurements of the two systems. However, our experiments show that this will have negligible impact on the successive growth steps.

With metallization, a shift of ∼0.3 eV can be seen in the components C−Si and Si−C, indicating a charge transfer to the surface SiC from the overlaying metal. Annealing to 450 °C and then 550 °C gives rise to new components in the Si 2p regions at binding energies of 98.0−100.5 eV. Similar features have been reported previously and associated with the formation of transition metal silicide phases.[19,31−35] Second, an attenuation and broadening are observed in the transition metal core levels Ru 3d and Fe 3p (the latter is not shown). Both indicate a reaction between the metallic thin films and the underlying Si-rich layers. Third, an increasing signal from the higher binding energy component ("C sp^2" in Figure 1c) suggests that new species of carbon have been formed, consistent with the previously reported transition-metal-mediated liberation of C atoms from SiC that re-form into graphitic carbon.[19]

Additional thermal treatments to 650 and 700 °C reveal a continuation of the same trend in the C 1s core level, where the intensity of the sp^2 carbon and silicide components increase relative to the intensity of the substrate (SiC). To quantify the amount of graphitic carbon formed from the reaction, the C 1s region was deconvolved into peak components corresponding to C sp^2 and C−Si signal. For the Ru/SiC system, the Ru $3d_{5/2}$ was initially fitted and used to estimate and deduct the intensity of Ru $3d_{3/2}$ features at the appropriate binding energy in the region overlapping with the C 1s components (this will be discussed later). The development of the (C sp^2)/(C−Si) signal ratio with temperature is shown in Figure 1d: at 700 °C the C sp^2 signal is more than double that of the substrate C−Si.

Together with the newfound diffractive features from the Fe/SiC and Ru/SiC surfaces in Figures 1a and 1b, respectively,

https://dx.doi.org/10.1021/acs.jpcc.0c10870
J. Phys. Chem. C 2021, 125, 4243−4252

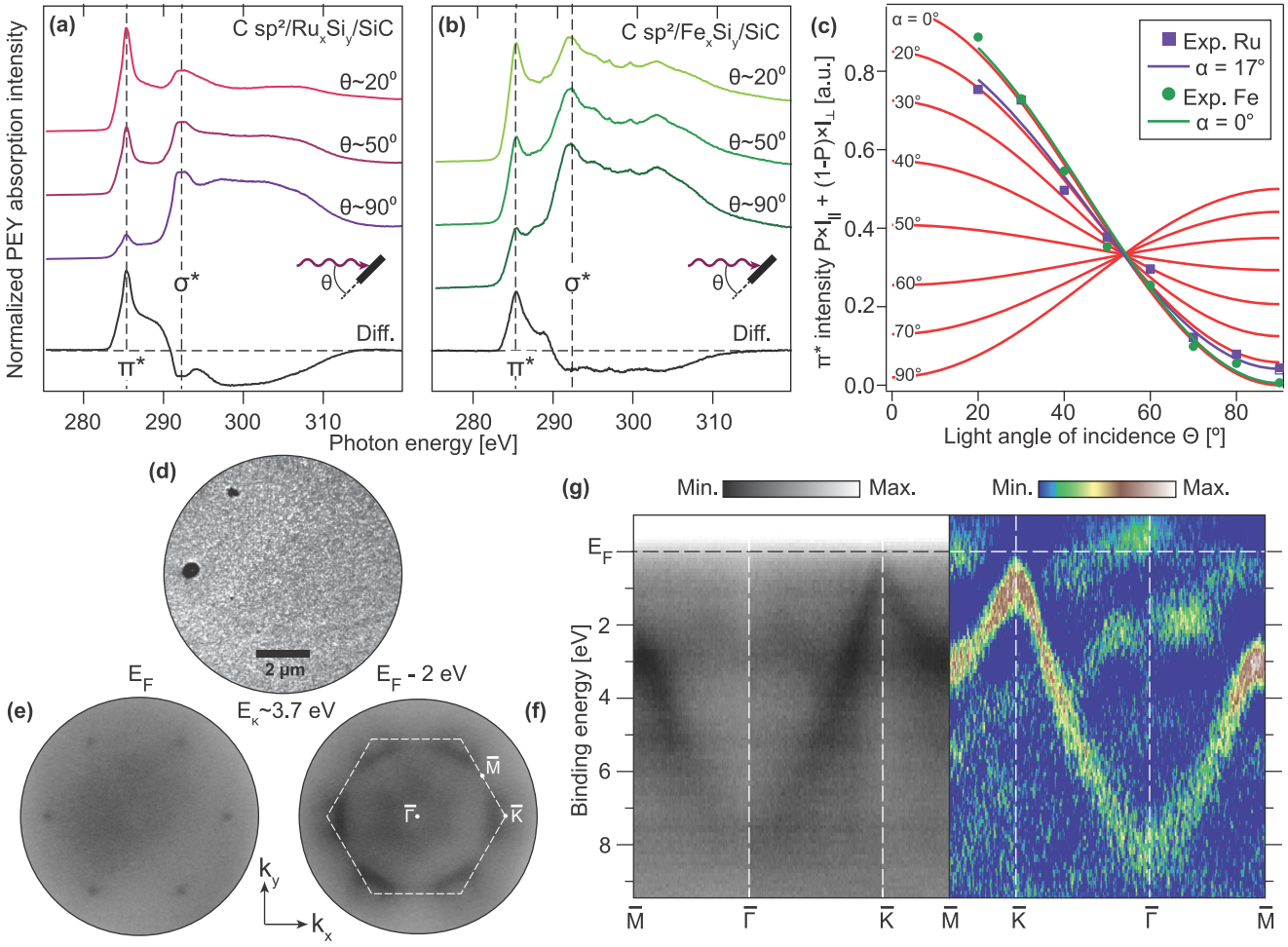

Figure 2. C 1s absorption spectra, layer orientation, and electronic structure of graphene. (a, b) Angle-dependent NEXAFS for graphene on Ru/SiC (a) and Fe/SiC (b) ranging from roughly grazing (~20°) to normal incidence. Prominent resonance features from the C 1s → π^* and C 1s → σ^* transitions can be seen at excitation energies 285.5 and 291.7 eV, respectively. A difference trace between the grazing and normal incidence spectra is also shown for each system to highlight the intensity changes with the light orientation. (c) Intensities of the LUMO (1s → π^*) absorption of graphene grown on Ru/SiC (purple) and Fe/SiC (green), plotted against the theoretical curves $I(\theta,\alpha)$ as described in eq 1. A best fit to each data set gives average angles $\alpha < 20°$ between the substrate surface normal and the vector perpendicular to the graphene layers. (d) LEEM micrograph (electron kinetic energy 3.7 eV) of the Fe/SiC surface following the formation of metal-mediated graphene at 600 °C. (e, f) Constant E vs ($\mathbf{k}_x$, $\mathbf{k}_y$) surfaces from the graphene in (d), measured at E_F (e) and $E_F - 2$ eV (f) with an excitation energy of $h\nu = 115$ eV. The first Brillouin zone boundary (dashed line) and high symmetry points $\bar{\Gamma}$, $\bar{M}$, and $\bar{K}$ have been marked. (g) E vs $\mathbf{k}_{||}$ intensity plots of occupied states in the gra/Fe/SiC system along principal directions $\bar{M} \rightarrow \bar{\Gamma}$, $\bar{\Gamma} \rightarrow \bar{K}$, and $\bar{K} \rightarrow \bar{M}$. The plot on the left shows the background-corrected band structure, while the plot on the right shows a second-derivative image (SDI), with a moderate boxcar averaging applied to amplify the graphene energy dispersion relative to the background.

and the mentioned attenuation of signals Ru 3d and Fe 3p, the results in Figure 1d indicate the formation of graphitic carbon on both metals at temperatures around 550 °C and higher. Similar results have been reported previously on the surfaces of bulk Ru[10] and Fe thin films,[19,20] where the precipitation of carbon is linked to the finite and temperature-dependent solubility of interstitial carbon in the two transition metals. Below 1000 °C, carbon is by far more soluble in Fe than in Ru.[36,37] The interstitial solubility in Ru is also expected to be highly temperature dependent. Addition of Si as a second alloying element has been shown to affect the carbon solubility in Fe.[38] Finally, the amount of carbon released from the chemical reaction between each metal and SiC will be dependent on the stoichiometry of the resultant silicide phase(s). It is therefore not surprising that similar thermal treatments for equally thick Fe and Ru films on SiC yield different amounts of graphitic surface carbon.

Near-edge X-ray absorption fine structure (NEXAFS) measurements of the C 1s K-edge from the Ru/SiC and Fe/SiC systems are presented in Figures 2a and 2b, respectively. The spectra were recorded from samples similar to those in Figure 1 before and after thermal treatments to 800 °C by using linearly polarized light at angles ranging from grazing (~20°) to normal incidence relative to the SiC(0001) plane. In both cases the annealing leads to new absorption resonances appearing at excitation energies 285.5 and 291.7 eV. While the latter indicates the existence of antibonding orbitals which overlap head-on (σ^*), the former is a fingerprint of antibonding p_z orbitals in sp^2-hybridized carbon, perpendicularly oriented to an aromatically configured macromolecular plane.[39,40] Hence, the strong 1s → π^* resonance supports the formation of new graphitic carbon on the samples.

The π^* resonances in Figure 2 also reveal a definite angle dependence, with stronger intensities observed when electrons

https://dx.doi.org/10.1021/acs.jpcc.0c10870
J. Phys. Chem. C 2021, 125, 4243−4252

are exited by light near grazing incidence to the samples. This suggests a prominent geometric ordering in the layers.[41] To determine the orientation of the C−C bonds relative to the plane of the SiC substrate, we compared the intensity of the lowest unoccupied molecular orbital (LUMO) excitation to an analytical solution of the NEXAFS intensity outlined by Stöhr and Outka.[42,43] Essentially, for carbon systems of 3-fold or higher symmetries, the resonance intensity of the 1s → π^* transition, when excited by linearly polarized light, can be reduced to

$$I \propto P\left(\cos^2\theta\,\cos^2\alpha + \frac{1}{2}\sin^2\theta\,\sin^2\alpha\right) + \frac{1-P}{2}\sin^2\alpha \quad (1)$$

where P is the polarization factor of the light hitting the sample plane at angle θ. The angle α between the sample surface normal and the vector perpendicular to the molecular plane of the inherent C−C bonds can thus be used to determine the average orientation of the graphitic planes on the surface.

In Figure 2c, the recorded LUMO intensities for the carbon in both material systems are plotted against the theoretical curves given by eq 1 for light with nearly perfect linear polarization ($P > 0.9$). To establish the angular intensity from the newly formed C−C carbon alone, a Gaussian profile was fitted to the π^* absorption feature for incidence angles θ = 20°−90°, and the background intensity of the clean SiC surface was subsequently deducted from the region. For the Ru/SiC system an additional, but presumably not angularly dependent, constant intensity offset was added to the Gaussians to account for any excitations from the Ru 3d state.

In the case of Fe/SiC, the measured average tilt angle α suggests that the graphene is precisely parallel to the substrate. For the Ru/SiC, the analysis reveals a larger tilt of roughly 17°, indicating that the graphene and its underlying layers are only more or less parallel. The reason for the larger α of Ru/SiC remains unclear but could be due to roughness at the interface, misalignment of the sample, or potentially other contributing factors.

To address the homogeneity of the sample surface, real-space analysis was also performed with LEEM. A surface micrograph from an Fe/SiC sample upon graphene formation at 600 °C is shown in Figure 2d. For low kinetic energies of the scattered electrons ($E_k \sim 3.7$ eV), the surface appears to be roughly uniform across ranges of 10+ μm. Only occasional submicrometer defects originating from the initial SiC surface can be seen. This suggests that on the given length scale coherent properties of the newfound graphene layers should be expected.

Next, the occupied electronic structure of the graphene was investigated with μ-ARPES. Measurements were performed on selected areas with 1.5 μm diameter, near the surface shown in Figure 2d and within the surrounding 50+ μm. The recorded band structures were compared with respect to doping induced by the substrate and variations in the number of graphene layers formed (if any).[26,44−46] In Figures 2e−g, a representative set of band structure measurements are shown. Two-dimensional plots of the electronic structure in reciprocal space ($\mathbf{k}_x$ vs $\mathbf{k}_y$) at constant energies relative to the Fermi level (E_F) are shown in Figures 2e and 2f. Near E_F, six distinguishable features from the π bands, i.e., Dirac "cones", appear at the $\bar{K}$ and $\bar{K}'$ points of the Brillouin zone. At 2 eV below E_F, another broad, hexagonal feature of smaller $\mathbf{k}$ values and with a 30° relative rotation can be seen.

In Figure 2g, the photoelectron intensity from the occupied states has been extracted for E vs $\mathbf{k}_\parallel$ along the principal symmetry directions of the surface Brillouin zone. Two similar plots are shown, where one (left) is the signal extracted from the constant energy surfaces and the other (right) is a second differential image (SDI) of the same signal with a moderate boxcar averaging applied. In both plots, the characteristic, near linearly dispersive bands of graphene are present around $\bar{K}$, indicating that at least one surface layer of graphene was formed from the reaction. The zero density of states crossing, i.e., the Dirac "point" E_D, is situated close to the Fermi level. This confirms the graphene not to be strongly doped from interactions with the underlying metal; however, weak doping cannot be ruled out within the resolution limits of the instrument (see the Supporting Information). Nonetheless, the measurements in Figures 2e−g agree with the literature,[10,19,20] in which a second layer of precipitated carbon from metals Fe and Ru will form quasi-freestanding graphene. The SDI in Figure 2g also reveals some additional, low $\mathbf{k}$ dispersive features around the $\bar{\Gamma}$ point at roughly 2 eV binding energy. The exact origin of these bands is uncertain but are assumed to arise from the metal's shallow d states and their interaction with the SiC surface.

With subsequent annealing to higher temperatures, both the gra/Fe/SiC and gra/Ru/SiC systems experience further changes to their structural composition (Figure 3). Not surprisingly, the relative intensity of graphene to SiC signal increases (Figure 1d), suggesting more metal has reacted with the SiC and liberated more carbon. Second, the signal intensity ratio between the two underlying layers, i.e., the metal (Fe or Ru) and the SiC substrate, shows a relatively higher proportion of SiC signal in the surface layers with increasing temperature (Figure 3a). After two short heat treatments to higher temperatures of 700 and 800 °C, the relative concentration of metal to SiC is <50% of the initial value. With any attenuation from the newfound graphene accounted for, these results suggest that the metal is in fact disappearing from the surface layers. Similar behavior was observed for intercalated adatoms of Fe[21,47] and Yb[48] at temperatures beyond 600 °C. The attenuation of Fe was explained by a temperature-driven diffusion into the underlying semiconductor substrate, and the same argument could easily be extended to Ru.

Assuming the metal is depleted from the surface layers by thermal diffusion, one could expect that probing deeper into the samples would reveal a relatively stronger XPS intensity from the diffused metallic species. In Figure 4, the C 1s regions of the gra/Fe/SiC and gra/Ru/SiC samples from Figure 3 are shown, but now probed with increasingly higher photo-excitation energies. Higher $h\nu$ gives longer inelastic mean-free paths λ for the excited photoelectrons, and so a signal from an increasingly thick slab of substrate material is being detected as $h\nu$ increases. In Figure 4a the C 1s of the gra/Fe/SiC, recorded with three selected photoexcitation energies corresponding to $\lambda \sim 0.5$ nm (surface sensitive), $\lambda \sim 0.9$ nm (moderately surface sensitive), and $\lambda \sim 1.6$ nm (substrate sensitive), is shown. The signal can be deconvolved into two main features at 282.9 and 284.3 eV. The former matches the binding energy of the previously observed SiC component, lowered by 0.3 eV due to interactions with the transition metal. The second feature is found at a binding energy roughly 0.1 eV lower than what is expected for neutral graphite and has a distinct asymmetric shape indicating a metallic surface nature.[14,15] At high surface sensitivity ($\lambda \sim 0.5$ nm), the sharp asymmetric feature

https://dx.doi.org/10.1021/acs.jpcc.0c10870
J. Phys. Chem. C 2021, 125, 4243−4252

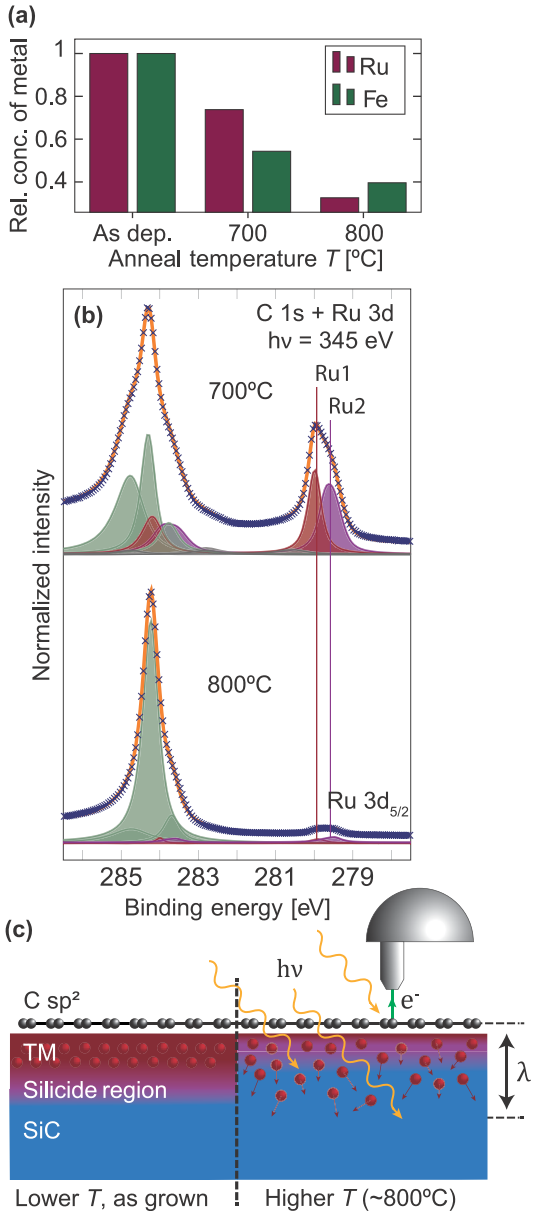

Figure 3. Diffusion of metal into the growth substrate. (a) Relative concentration of metal in the surface layers before and after high-temperature annealing. The measure of the metal content is given as the ratio of Ru and Fe core level signal to the substrate carbon signal, corrected for differences in cross sections and normalized to unity after deposition (room temperature). Diffusion into the SiC substrate is evident from the treatments to subsequently higher temperatures. (b) C 1s and Ru 3d core levels of the gra/Ru/SiC system, measured with photon energy $h\nu$ = 345 eV after subsequent heat treatments to 700 °C and then 800 °C. (c) Schematic of metal diffusion into the substrate of the SiC substrate during annealing to 800 °C.

dominates the intensity of the region, but at lower surface sensitivity ($\lambda \rightarrow 1.6$ nm) the weight is shifted toward the substrate peak. This matches well with the notion of a finite amount of graphene situated at the surface: at low λ most of the C 1s signal comes from the layers of sp^2 carbon, but at higher λ more substrate layers are added to the probing region and so the SiC signal dominates. The familiar 0.3 eV energy shift of the C−Si component (see Figure 1c) may indicate that the surface layers have been doped by the Fe and that the same doping level persists even after higher temperature annealing. On the other hand, the small (0.1 eV) energy shift of the C sp^2 component indicates only weak doping of the graphene, consistent with what was observed from the band structure in Figure 2g and other systems.[10,19,20]

In Figure 4d, the same exercise is repeated for gra/Ru/SiC with the same photoexcitation energies. Note that the deconvolution is more complicated due to the overlapping C 1s and Ru 3d signals. However, from the known energy separation and intensity ratio of the $3d_{5/2}$ and $3d_{3/2}$ signals, one can accurately determine the components of Ru $3d_{3/2}$ based on those observed in the Ru $3d_{5/2}$ region. The overlapping C 1s and Ru $3d_{3/2}$ signal was thus deconvolved by placing features of the bare SiC and the predetermined Ru components together and adding the minimum number of additional features to optimize the fit.

Not surprisingly, the same distinct asymmetric feature seen in Figure 4a is also visible for gra/Ru/SiC in Figure 4d, now at 284.2 eV. Near the surface ($\lambda \sim 0.5$ nm) the SiC feature cannot be seen, but with increasing λ it again becomes visible at lower binding energy 282.8 eV. This indicates that within ±0.1 eV the doping from the Ru is similar to what was observed from the Fe in Figure 4a.

At moderate depth sensitivity, the Ru contributes with two distinct features: one at 280.0 eV (Ru1) corresponding to that of metallic Ru[49,50] and one at 0.4 eV lower binding energy (Ru2) matching with that observed for Ru silicides.[34,35,51] With increasing depth sensitivity, the relative weight of the two changes and new Ru features become visible at higher binding energies (Ru3). This indicates that different Ru species are present at different depths into the substrate, in line with the thermally activated diffusion of metal into the substrate that was shown in Figure 3.

Note that for the thermal treatments in Figure 4 the metal signal in the surface layers is reduced but not fully diminished. While the graphene (C sp^2) appear to be only weakly doped and thus ultimately not very affected, any metal impurities present in the SiC can work to reduce electron and hole mobility of the substrate. This may or may not be a potential concern for applications where the underlying semiconductor plays an active role, for example, in graphene-based field effect transistors (GFETs). A proper understanding of the impact of residual metal impurities in the SiC would require further investigations that are beyond the scope of this work.

To correctly determine the position of the graphene layers relative to the metal silicide and the SiC, the C 1s intensity was extracted for additional photoexcitation energies in the range 315−1200 eV. In Figure 4b, the variation of the graphene intensity relative to the total accumulated intensity within the scan regions of both material systems is shown. In the gra/Fe/SiC system the relative graphene intensity was estimated by first deconvolving the C 1s region and then comparing the sum of the asymmetric feature at 284.3 eV and the surface peaks (S1, S2) to the total signal. For the gra/Ru/SiC, the graphene signal was estimated by first determining the total Ru $3d_{5/2}$ intensity, calculating the Ru $3d_{3/2}$ intensity based on their known ratio, and deducting both of these intensities from the scan region. Note that for simplicity in the Ru case the total C 1s intensity was assumed to come from graphene, as the deconvolution in Figure 4d revealed the SiC signal from the substrate to be negligible except when using the very highest ($h\nu$ > 800 eV) photoexcitation energies. Both systems show a negative exponential decay in graphene intensity with increasing $h\nu$, as expected from Beer−Lambert's law for a

https://dx.doi.org/10.1021/acs.jpcc.0c10870
J. Phys. Chem. C 2021, 125, 4243−4252

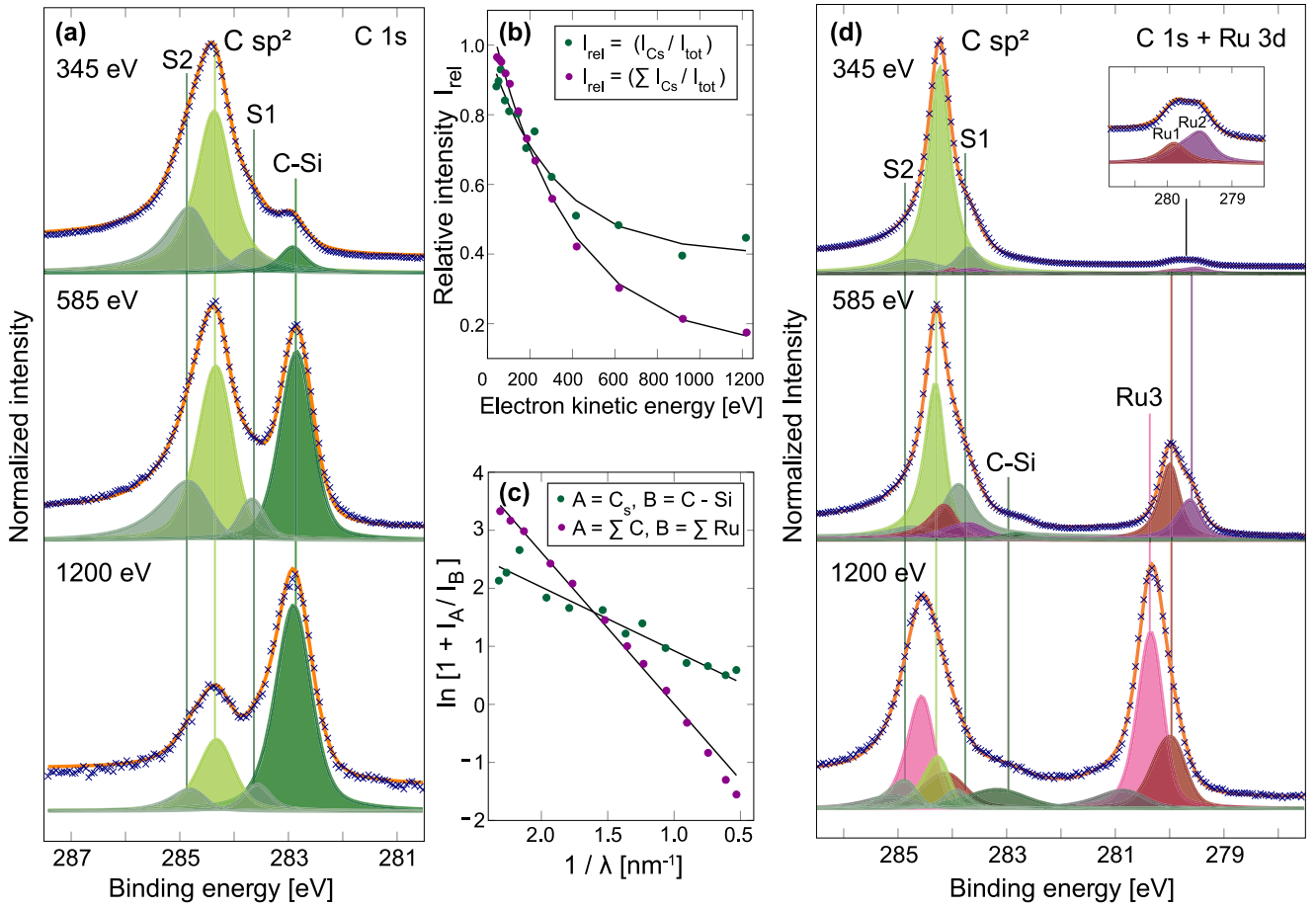

Figure 4. Depth profiling of graphene from mediated growth using Fe and Ru on SiC. (a, d) A selection of C 1s core level spectra from samples covered with Fe and Ru, respectively, after annealing to 800 °C. The three core levels in each set were measured with photon energies $h\nu$ = 345 eV (surface sensitive), $h\nu$ = 585 eV (moderately surface sensitive), and $h\nu$ = 1200 eV (substrate sensitive). (b) A full range of data points for the photoelectron intensity of graphene (I_{Cs}) relative to the total intensity (I_{tot}) from the energy regions in (a) and (d) as a function of kinetic energy for the exited photoelectrons. Note that the two data sets differ slightly in their normalizations, with green (gra/Fe/SiC) stating the fractional intensity of C sp^2 plus surface peaks (S1, S2), while for purple (gra/Ru/SiC) all carbon features were assumed to be surface carbon for simplicity. (c) The data from (b), replotted to show the relationship between the relative photoelectron intensity and the inverse inelastic mean-free path λ from a simple two-layer model: surface graphene (I_A) on top of an underlying and metal-rich substrate region (I_B). An evident linearity can be seen from the data, similar to that of the ideal two-layer model. As seen from (a) and (d) the Ru signal, but not Fe signal, can be seen in the relevant energy regions of the C 1s core level. Hence, for the gra/Fe/SiC system, the C sp^2 intensities (top layer) are compared to the carbon signal from the underlying SiC substrate (bottom layer), while for the gra/Ru/SiC system the metallic Ru signal is considered to be the bottom layer.

system with finite signal detected from the surface layers. On the basis of these observations, we used a simple two-layer model to determine the thickness of the graphene layers, assuming these to be residing on top of underlying transition metal and SiC. For each photoexcitation energy, the signal from surface carbon I_s was compared to the signal assigned to the underlying layers I within the same scan region, according to

$$\frac{d}{\lambda} = \ln\left[1 + \frac{I\sigma_s}{I_s\sigma}\right] \quad (2)$$

where σ_s and σ are the photoexcitation cross-sections for the topmost and lowermost layers, respectively, and d is the estimated thickness of the carbon overlayer. The total surface carbon signal of the gra/Fe/SiC system was thus compared to that of the underlying SiC substrate, while for the gra/Ru/SiC system, the total C 1s signal was compared to that of the underlying Ru. In Figure 4c, it is shown that a linear relationship between the logarithm in eq 2 and the inverse inelastic mean-free path is obtained for both material systems. This is in accordance with the assumed layer structure from the simplified two-layer model. The gradient from the best fit of each data set gives an estimate of the thickness d of the graphene overlayers: 1.1 and 2.6 nm are obtained for the two systems gra/Fe/SiC and gra/Ru/SiC, respectively. If one assumes that the graphene layers are weakly bound together by van der Waals forces with an interlayer spacing equal to that of graphite (0.355 nm),[52] then roughly 3−8 layers have been formed, regulated by the applied temperature and the thickness of the mediating metal deposited.

CONCLUSIONS

The metal-mediated growth of epitaxial few-layer graphene on the surface of 6H-SiC(0001) treated with Fe or Ru has been investigated, at a temperature far lower than that required for graphene growth directly from the SiC crystal. Using surface diffraction and surface sensitive photoemission measurements, we observed the onset of graphene formation after short thermal treatments to 450 °C, and the familiar electronic

https://dx.doi.org/10.1021/acs.jpcc.0c10870
J. Phys. Chem. C 2021, 125, 4243−4252

structure of graphene was confirmed for the newly formed species at 600 °C by using ARPES. Further annealing to higher temperatures of 700−800 °C revealed the formation of additional graphene layers (3−8 layers). Both metals were seen to produce either neutral or weakly doped, quasi-freestanding multilayer graphene. The placement of the graphene near the sample surface and its parallel orientation relative to the underlying growth substrate were established from depth sensitive photoemission and angle-dependent absorption spectroscopy measurements, respectively. The tunable depth sensitivity of the photoemission measurements was also used to confirm that the mediating metal agents, Fe and Ru, can be made to diffuse into the SiC crystal with subsequent thermal treatments to higher temperatures.

From these investigations we have established a modified recipe for graphene production requiring a minimal number of processing steps. The controllable growth of high quality, few-layer graphene-on-semiconductor has been achieved at industrially compatible temperatures that so far have not been available by using other, more conventional growth techniques. The number of graphene layers formed is limited by the type and thickness of the transition metal film and the temperatures to which the material system is subjected. The option to use either Fe or Ru interchangeably over a range of different temperatures allows graphene with a tunable thickness to be formed. The possibility to diffuse the mediating metal agents into the substrate means graphene can be supported either on magnetic silicide layers or directly on SiC, as required. This makes metal-mediated graphene growth a realistic and promising candidate for realizing graphene-based devices within the pre-existing framework of large-scale device processing.

■ ASSOCIATED CONTENT

Supporting Information

The Supporting Information is available free of charge at https://pubs.acs.org/doi/10.1021/acs.jpcc.0c10870.

Additional details regarding the experimental setup as well as relevant experimental parameters for the results presented in the text and in Figures 1−4 (PDF)

■ AUTHOR INFORMATION

Corresponding Authors

Håkon I. Røst − *Center for Quantum Spintronics, Department of Physics, Norwegian University of Science and Technology (NTNU), NO-7491 Trondheim, Norway;* orcid.org/0000-0002-1853-8349; Email: hakon.i.rost@ntnu.no

Rajesh Kumar Chellappan − *Center for Quantum Spintronics, Department of Physics, Norwegian University of Science and Technology (NTNU), NO-7491 Trondheim, Norway*; Email: rajesh.k.chellappan@ntnu.no

Justin W. Wells − *Center for Quantum Spintronics, Department of Physics, Norwegian University of Science and Technology (NTNU), NO-7491 Trondheim, Norway;* orcid.org/0000-0001-6366-366X; Email: justin.wells@ntnu.no

Authors

Frode S. Strand − *Center for Quantum Spintronics, Department of Physics, Norwegian University of Science and Technology (NTNU), NO-7491 Trondheim, Norway*

Antonija Grubišić-Čabo − *School of Physics & Astronomy, Monash University, Clayton, Victoria 3168, Australia;* orcid.org/0000-0001-7683-0295

Benjamen P. Reed − *Department of Physics, Aberystwyth University, Aberystwyth SY23 3BZ, United Kingdom*

Mauricio J. Prieto − *Department of Interface Science, Fritz-Haber-Institute of the Max-Planck Society, 14195 Berlin, Germany;* orcid.org/0000-0002-5087-4545

Liviu C. Tănase − *Department of Interface Science, Fritz-Haber-Institute of the Max-Planck Society, 14195 Berlin, Germany;* orcid.org/0000-0002-4177-5676

Lucas de Souza Caldas − *Department of Interface Science, Fritz-Haber-Institute of the Max-Planck Society, 14195 Berlin, Germany*

Thipusa Wongpinij − *Synchrotron Light Research Institute, Nakhon Ratchasima 30000, Thailand*

Chanan Euaruksakul − *Synchrotron Light Research Institute, Nakhon Ratchasima 30000, Thailand*

Thomas Schmidt − *Department of Interface Science, Fritz-Haber-Institute of the Max-Planck Society, 14195 Berlin, Germany;* orcid.org/0000-0003-4389-2080

Anton Tadich − *Australian Synchrotron, Clayton, Victoria 3168, Australia*

Bruce C. C. Cowie − *Australian Synchrotron, Clayton, Victoria 3168, Australia*

Zheshen Li − *Department of Physics and Astronomy, Aarhus University, 8000 Aarhus C, Denmark*

Simon P. Cooil − *Department of Physics, Aberystwyth University, Aberystwyth SY23 3BZ, United Kingdom; Semiconductor Physics, Department of Physics, University of Oslo (UiO), NO-0371 Oslo, Norway;* orcid.org/0000-0002-0856-6020

Complete contact information is available at: https://pubs.acs.org/10.1021/acs.jpcc.0c10870

Notes

The authors declare no competing financial interest.

■ ACKNOWLEDGMENTS

This work was partly supported by the Research Council of Norway through its Centres of Excellence funding scheme, project number 262633 "QuSpin", through project number 250555/O70 "GraSeRad", and through the Norwegian Micro- and Nano-Fabrication Facility, NorFab, project number 245963/F50. The SMART instrument was financially supported by the Federal German Ministry of Education and Research (BMBF) under the contract 05KS4WWB/4, as well as by the Max-Planck Society. Parts of this research was undertaken on the UE49-PGM-SMART beamline at BESSYII, the Synchrotron Light Research Institute (SLRI) in Thailand, and on the soft X-ray spectroscopy beamline at the Australian Synchrotron, part of ANSTO. We thank both the Helmholtz-Center Berlin for Materials and Energy (HZB), SLRI and ANSTO for the allocation of beamtime. S.P.C. would like to acknowledge the European Regional Development Fund (ERDF) and the Welsh European Funding Office (WEFO) for funding the second Solar Photovoltaic Academic Research Consortium (SPARC II). B.P.R. acknowledges the EPSRC CDT in Diamond Science and Technology. L.d.S.C. is grateful for the funding through the Deutsche Forschungsgemeinschaft (DFG, German Research Foundation) under Germany's Excellence Strategy-EXC 2008-390540038 (UniSysCat).

https://dx.doi.org/10.1021/acs.jpcc.0c10870
J. Phys. Chem. C 2021, 125, 4243−4252

H.I.R., J.W.W. and S.P.C. would also like to thank Dr. Mark Edmonds, Dr. Federico Mazzola and Dr. Andrew Evans for fruitful discussions.

REFERENCES

(1) Novoselov, K. S.; Geim, A. K.; Morozov, S. V.; Jiang, D.; Zhang, Y.; Dubonos, S. V.; Grigorieva, I. V.; Firsov, A. A. Electric field effect in atomically thin carbon films. *Science* **2004**, *306*, 666−669.
(2) Bolotin, K. I.; Sikes, K. J.; Jiang, Z.; Klima, M.; Fudenberg, G.; Hone, J.; Kim, P.; Stormer, H. Ultrahigh electron mobility in suspended graphene. *Solid State Commun.* **2008**, *146*, 351−355.
(3) Neto, A. C.; Guinea, F.; Peres, N. M.; Novoselov, K. S.; Geim, A. K. The electronic properties of graphene. *Rev. Mod. Phys.* **2009**, *81*, 109.
(4) Balandin, A. A. Thermal properties of graphene and nanostructured carbon materials. *Nat. Mater.* **2011**, *10*, 569−581.
(5) Falkovsky, L. Optical properties of graphene. *J. Phys. Conf. Ser.* **2008**, *129*, 012004.
(6) Papageorgiou, D. G.; Kinloch, I. A.; Young, R. J. Mechanical properties of graphene and graphene-based nanocomposites. *Prog. Mater. Sci.* **2017**, *90*, 75−127.
(7) Varykhalov, A.; Sánchez-Barriga, J.; Shikin, A. M.; Biswas, C.; Vescovo, E.; Rybkin, A.; Marchenko, D.; Rader, O. Electronic and Magnetic Properties of Quasifreestanding Graphene on Ni. *Phys. Rev. Lett.* **2008**, *101*, 157601.
(8) N'Diaye, A. T.; Bleikamp, S.; Feibelman, P. J.; Michely, T. Two-dimensional Ir cluster lattice on a graphene Moiré on Ir(111). *Phys. Rev. Lett.* **2006**, *97*, 215501.
(9) Sutter, P.; Sadowski, J. T.; Sutter, E. Graphene on Pt (111): Growth and substrate interaction. *Phys. Rev. B: Condens. Matter Mater. Phys.* **2009**, *80*, 245411.
(10) Sutter, P. W.; Flege, J.-I.; Sutter, E. A. Epitaxial graphene on ruthenium. *Nat. Mater.* **2008**, *7*, 406−411.
(11) Berger, C.; Song, Z.; Li, T.; Li, X.; Ogbazghi, A. Y.; Feng, R.; Dai, Z.; Marchenkov, A. N.; Conrad, E. H.; First, P. N.; et al. Ultrathin epitaxial graphite: 2D electron gas properties and a route toward graphene-based nanoelectronics. *J. Phys. Chem. B* **2004**, *108*, 19912−19916.
(12) Hass, J.; Feng, R.; Li, T.; Li, X.; Zong, Z.; De Heer, W.; First, P.; Conrad, E.; Jeffrey, C.; Berger, C. Highly ordered graphene for two dimensional electronics. *Appl. Phys. Lett.* **2006**, *89*, 143106.
(13) Coraux, J.; N'Diaye, A. T.; Busse, C.; Michely, T. Structural coherency of graphene on Ir (111). *Nano Lett.* **2008**, *8*, 565−570.
(14) Emtsev, K.; Speck, F.; Seyller, T.; Ley, L.; Riley, J. D. Interaction, growth, and ordering of epitaxial graphene on SiC {0001} surfaces: A comparative photoelectron spectroscopy study. *Phys. Rev. B: Condens. Matter Mater. Phys.* **2008**, *77*, 155303.
(15) Emtsev, K. V.; Bostwick, A.; Horn, K.; Jobst, J.; Kellogg, G. L.; Ley, L.; McChesney, J. L.; Ohta, T.; Reshanov, S. A.; Röhrl, J.; et al. Towards wafer-size graphene layers by atmospheric pressure graphitization of silicon carbide. *Nat. Mater.* **2009**, *8*, 203−207.
(16) Zhang, Z.; Du, J.; Zhang, D.; Sun, H.; Yin, L.; Ma, L.; Chen, J.; Ma, D.; Cheng, H.-M.; Ren, W. Rosin-enabled ultraclean and damage-free transfer of graphene for large-area flexible organic light-emitting diodes. *Nat. Commun.* **2017**, *8*, 1−9.
(17) Lin, Y.-M.; Dimitrakopoulos, C.; Jenkins, K. A.; Farmer, D. B.; Chiu, H.-Y.; Grill, A.; Avouris, P. 100-GHz transistors from wafer-scale epitaxial graphene. *Science* **2010**, *327*, 662−662.
(18) Aliofkhazraei, M.; Ali, N.; Milne, W. I.; Ozkan, C. S.; Mitura, S.; Gervasoni, J. L. *Graphene Science Handbook: Electrical and Optical Properties*; CRC Press: 2016; Chapter 1, pp 5−6.
(19) Cooil, S.; Song, F.; Williams, G.; Roberts, O.; Langstaff, D.; Jørgensen, B.; Høydalsvik, K.; Breiby, D.; Wahlström, E.; Evans, D.; et al. Iron-mediated growth of epitaxial graphene on SiC and diamond. *Carbon* **2012**, *50*, 5099−5105.
(20) Cooil, S.; Wells, J.; Hu, D.; Niu, Y.; Zakharov, A.; Bianchi, M.; Evans, D. Controlling the growth of epitaxial graphene on metalized diamond (111) surface. *Appl. Phys. Lett.* **2015**, *107*, 181603.
(21) Shen, K.; Sun, H.; Hu, J.; Hu, J.; Liang, Z.; Li, H.; Zhu, Z.; Huang, Y.; Kong, L.; Wang, Y.; et al. Fabricating quasi-free-standing graphene on a SiC (0001) surface by steerable intercalation of iron. *J. Phys. Chem. C* **2018**, *122*, 21484−21492.
(22) Kern, W. The evolution of silicon wafer cleaning technology. *J. Electrochem. Soc.* **1990**, *137*, 1887−1892.
(23) Starke, U.; Bernhardt, J.; Schardt, J.; Heinz, K. SiC surface reconstruction: Relevancy of atomic structure for growth technology. *Surf. Rev. Lett.* **1999**, *6*, 1129−1141.
(24) Starke, U.; Schardt, J.; Bernhardt, J.; Franke, M.; Heinz, K. Stacking transformation from hexagonal to cubic SiC induced by surface reconstruction: A seed for heterostructure growth. *Phys. Rev. Lett.* **1999**, *82*, 2107−2110.
(25) Starke, U.; Riedl, C. Epitaxial graphene on SiC(0001) and SiC(): From surface reconstructions to carbon electronics. *J. Phys.: Condens. Matter* **2009**, *21*, 134016.
(26) Ohta, T.; Bostwick, A.; Seyller, T.; Horn, K.; Rotenberg, E. Controlling the electronic structure of bilayer graphene. *Science* **2006**, *313*, 951−954.
(27) Nakao, A.; Iwaki, M.; Sakairi, H.; Terasima, K. XPS characterization of nitrogen implanted silicon carbide. *Nucl. Instrum. Methods Phys. Res., Sect. B* **1992**, *65*, 352−356.
(28) Wang, Y.-Y.; Kusumoto, K.; Li, C.-J. XPS analysis of SiC films prepared by radio frequency plasma sputtering. *Phys. Procedia* **2012**, *32*, 95−102.
(29) Hollinger, G.; Himpsel, F. Probing the transition layer at the SiO_2-Si interface using core level photoemission. *Appl. Phys. Lett.* **1984**, *44*, 93−95.
(30) Watanabe, H.; Hosoi, T.; Kirino, T.; Kagei, Y.; Uenishi, Y.; Chanthaphan, A.; Yoshigoe, A.; Teraoka, Y.; Shimura, T. Synchrotron X-ray photoelectron spectroscopy study on thermally grown SiO_2/4H-SiC (0001) interface and its correlation with electrical properties. *Appl. Phys. Lett.* **2011**, *99*, 021907.
(31) Rührnschopf, K.; Borgmann, D.; Wedler, G. Growth of Fe on Si (100) at room temperature and formation of iron silicide. *Thin Solid Films* **1996**, *280*, 171−177.
(32) Gomoyunova, M.; Malygin, D.; Pronin, I.; Voronchikhin, A.; Vyalikh, D.; Molodtsov, S. Initial stages of iron silicide formation on the Si(100) 2 × 1 surface. *Surf. Sci.* **2007**, *601*, 5069−5076.
(33) Wang, Z.-J.; Dong, A.; Wei, M.; Fu, Q.; Bao, X. Graphene as a surfactant for metal growth on solid surfaces: Fe on graphene/SiC (0001). *Appl. Phys. Lett.* **2014**, *104*, 181604.
(34) Lu, Z.; Sham, T.; Norton, P.; Tan, K. Photoemission studies of silicon on the Ru (001) surface. *Appl. Phys. Lett.* **1991**, *58*, 161−163.
(35) Lizzit, S.; Larciprete, R.; Lacovig, P.; Dalmiglio, M.; Orlando, F.; Baraldi, A.; Gammelgaard, L.; Barreto, L.; Bianchi, M.; Perkins, E.; et al. Transfer-free electrical insulation of epitaxial graphene from its metal substrate. *Nano Lett.* **2012**, *12*, 4503−4507.
(36) Zhukov, A. Phase diagram of alloys of the system Fe-C. *Met. Sci. Heat Treat.* **1988**, *30*, 249−255.
(37) Arnoult, W. J.; McLellan, R. B. Solubility of carbon in rhodium, ruthenium, iridium, and rhenium. *Scr. Metall.* **1972**, *6*, 1013−1018.
(38) Sanbongi, K.; Ohtani, M.; Toita, K. On the effect of alloying elements on the solubility of carbon in molten iron. *Sci. rep. Res. Inst., Tohoku Univ., Ser. A* **1957**, 147−158.
(39) Pacilé, D.; Papagno, M.; Rodríguez, A. F.; Grioni, M.; Papagno, L.; Girit, Ç.; Meyer, J.; Begtrup, G.; Zettl, A. Near-edge X-ray absorption fine-structure investigation of graphene. *Phys. Rev. Lett.* **2008**, *101*, 066806.
(40) Shpilman, Z.; Gouzman, I.; Minton, T.; Shen, L.; Stacey, A.; Orwa, J.; Prawer, S.; Cowie, B.; Hoffman, A. A near edge X-ray absorption fine structure study of oxidized single crystal and polycrystalline diamond surfaces. *Diamond Relat. Mater.* **2014**, *45*, 20−27.
(41) Kim, K.-J.; Lee, H.; Choi, J.; Lee, H.; Kang, T.; Kim, B.; Kim, S. Temperature dependent structural changes of graphene layers on 6H-SiC (0001) surfaces. *J. Phys.: Condens. Matter* **2008**, *20*, 225017.
(42) Stöhr, J.; Outka, D. Determination of molecular orientations on surfaces from the angular dependence of near-edge X-ray-absorption

https://dx.doi.org/10.1021/acs.jpcc.0c10870
J. Phys. Chem. C 2021, 125, 4243−4252

fine-structure spectra. *Phys. Rev. B: Condens. Matter Mater. Phys.* **1987**, *36*, 7891.
(43) Stöhr, J. *NEXAFS Spectroscopy*; Springer Science & Business Media: 2013; Vol. *25*; Chapter 9, pp 279−291.
(44) Bostwick, A.; Ohta, T.; Seyller, T.; Horn, K.; Rotenberg, E. Quasiparticle dynamics in graphene. *Nat. Phys.* **2007**, *3*, 36−40.
(45) Ohta, T.; Bostwick, A.; McChesney, J. L.; Seyller, T.; Horn, K.; Rotenberg, E. Interlayer interaction and electronic screening in multilayer graphene investigated with angle-resolved photoemission spectroscopy. *Phys. Rev. Lett.* **2007**, *98*, 206802.
(46) Siegel, D. A.; Hwang, C.; Fedorov, A. V.; Lanzara, A. Quasifreestanding multilayer graphene films on the carbon face of SiC. *Phys. Rev. B: Condens. Matter Mater. Phys.* **2010**, *81*, 241417.
(47) Sung, S.; Yang, J.; Lee, P.; Kim, J.; Ryu, M.; Park, H.; Lee, G.; Hwang, C.; Kim, K. S.; Kim, J.; et al. Spin-induced band modifications of graphene through intercalation of magnetic iron atoms. *Nanoscale* **2014**, *6*, 3824−3829.
(48) Watcharinyanon, S.; Johansson, L. I.; Xia, C.; Flege, J. I.; Meyer, A.; Falta, J.; Virojanadara, C. Ytterbium intercalation of epitaxial graphene grown on Si-face SiC. *Graphene* **2013**, *02*, 66−73.
(49) Fuggle, J.; Madey, T.; Steinkilberg, M.; Menzel, D. Photoelectron spectroscopic studies of adsorption of CO and oxygen on Ru (001). *Surf. Sci.* **1975**, *52*, 521−541.
(50) Kaga, Y.; Abe, Y.; Yanagisawa, H.; Kawamura, M.; Sasaki, K. Ru and RuO_2 thin films by XPS. *Surf. Sci. Spectra* **1999**, *6*, 68−74.
(51) Pasquali, L.; Mahne, N.; Montecchi, M.; Mattarello, V.; Nannarone, S. Formation and distribution of compounds at the Ru-Si (001) ultrathin film interface. *J. Appl. Phys.* **2009**, *105*, 044304.
(52) De Andres, P.; Ramírez, R.; Vergés, J. A. Strong covalent bonding between two graphene layers. *Phys. Rev. B: Condens. Matter Mater. Phys.* **2008**, *77*, 045403.

https://dx.doi.org/10.1021/acs.jpcc.0c10870
J. Phys. Chem. C 2021, 125, 4243−4252